Microporous Humins Synthesized in Concentrated Sulfuric Acid Using 5-Hydroxymethyl Furfural

N.B. When citing this work, cite the original published paper.

(article starts on next page)

Microporous Humins Synthesized in Concentrated Sulfuric Acid Using 5-Hydroxymethyl Furfural

Fredrik Björnerbäck, Diana Bernin,[†] and Niklas Hedin*

Department of Materials and Environmental Chemistry, Arrhenius Laboratory, Stockholm University, SE-106 91 Stockholm, Sweden

S *Supporting Information*

ABSTRACT: A new class of highly porous organic sorbents called microporous humins is presented. These microporous humins are derived from sustainable and industrially abundant resources, have high heat of CO_2 sorption, and could potentially be useful for the separation of carbon dioxide from gas mixtures. Their synthesis involves the polymerization of 5-hydroxymethyl furfural (HMF) in concentrated sulfuric acid and treatment with diethyl ether and heat. In particular, the porosities were tuned by the heat treatment. HMF is a potential platform chemical from biorefineries and a common intermediate in carbohydrate chemistry. A high uptake of CO_2 (up to 5.27 mmol/g at 0 °C and 1 bar) and high CO_2-over-N_2 and CO_2-over-CH_4 selectivities were observed. The microporous humins were aromatic and structurally amorphous, which was shown in a multipronged approach using ^{13}C nuclear magnetic resonance and Fourier transform infrared spectroscopies, elemental analysis, and wide-angle X-ray scattering.

HMF → H_2SO_4 →
1. 50 °C, 24 h
2. Diethyl ether wash
3. 200−400 °C, N_2-flow
→ Microporous humins
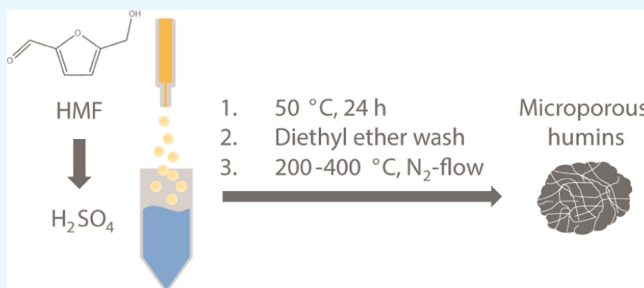
INTRODUCTION

The purpose of this study was to design a new class of organic microporous sorbents for CO_2 removal processes, using only industrially abundant and sustainable resources. As of today, many microporous sorbents are derived from petroleum products or include scarce elements. Consequently, efforts are being made to synthesize sorbents through more sustainable or renewable means.[1−3] It is established that carbon-rich materials can be synthesized using platform molecules of biorefineries.[4] 5-Hydroxymethylfurfural (HMF) is such a molecule,[5,6] which could also be used in fuel additives, as a monomer, and in the synthesis of other chemical derivatives.[5−7]

When sugars or biomass are converted to HMF and levulinic and formic acids, solid side products often form. These side products are called humins.[4,8] They have polymeric structures and their mechanism of formation has been studied in detail.[8] They have been related to the hydrochars or biocarbons that precipitate during hydrothermal carbonization (HTC) processes, in which HMF has been shown to be an intermediate reaction product.[9] The use of humins is thought to be limited to the generation of heat or as soil enhancers.[8] However, because of the complex, diverse, and relatively unknown structure[8] of humins, we see large potential in using them in material applications. For instance, humin-containing foams have been prepared.[10]

The reactions of sulfuric acid (H_2SO_4) with sugars have been studied for decades, and it is well established that humins form in such reactions.[11,12] Another documented use of H_2SO_4 is as an activation agent in the production of activated carbons

from biomass.[13] Although there are variations to the procedure, typically, biomass is impregnated with H_2SO_4 and subsequently heated in a N_2 atmosphere. Mechanistically, H_2SO_4 has been proposed to act as a dehydration catalyst during such activation.[14] H_2SO_4 can act as an acid catalyst during synthesis of carbon-based materials using silica templates. Hard templating of carbons using silica templates involves multiple steps and high temperatures and the carbons can have surface areas up to 2200 m^2/g.[15] Carbon films have also been produced from sucrose and H_2SO_4 using polystyrene spheres as templates.[16] H_2SO_4 has also been used as a reagent in HTC[17] of biomass and molecules and to produce sulfur-doped carbon dots from waste frying oil.[18]

As HMF could be a future platform chemical and is a common intermediate in carbohydrate chemistry, the objective of this study was to derive highly porous humins from it. We synthesized microporous humins with large surface areas and high levels of CO_2 uptake from HMF in conc. H_2SO_4.

RESULTS AND DISCUSSION

Microporous Humins from HMF. Microporous humins were synthesized by transferring atomized droplets of HMF to conc. H_2SO_4, subjecting the reactive system to successive treatment with diethyl ether, and a final heat treatment. The microporous humin derived from HMF at 400 °C (MHH-4) displayed higher specific surface area and pore volume than

that prepared at 200 °C MHH-2, as can be seen from Table 1. These differences appear to relate to heat-induced removal of

**Table 1. Textural Properties of MHH-2 and MHH-4[a]**

sample	S_{BET} (m²/g)	S_{EXT} (m²/g)	S_{mic} (m²/g)	V_t (cm³/g)	V_{mic} (cm³/g)
MHH-2	542	83	459	0.35	0.19
MHH-4	1019	174	845	0.73	0.35

[a]MHH-2 and MHH-4 denote sorbents derived from HMF at 200 and 400 °C, respectively. S_{BET}, S_{EXT}, and S_{mic} are the BET-specific, external, and micropore surface areas, respectively. V_t and V_{mic} denote total pore and micropore volumes, respectively.

small molecules. The yield for MHH-4 (40 wt %) was lower than that for MHH-2 (56 wt %). An additional valuable aspect of the procedure to synthesize the microporous humins was the high level of reproducibility. The corresponding CO_2 sorption isotherms for replicates of MHH-4 and MHH-2 are displayed in Figures S1 and S2.

The heat treatment was important for the microporosity as was the other steps of the procedure. Treatment or washing with a solvent is commonly used but seldom discussed and can be considered crucial for the extraction of molecules, for example, solvents, catalysts, monomers, dimers, and so forth, from an already formed polymer or polymer precursor.[19,20] However, diethyl ether appears not only to have extracted small molecules but also to have induced a phase separation which produced part of the solid phase of interest.

Molecular Analyses Revealed Largely Aromatic Structures. Conc. H_2SO_4 is an established oxidation and dehydration agent;[18] however, the position of MHH-2 in the van Krevelen diagram[21] of Figure 1 shows that it is not a direct
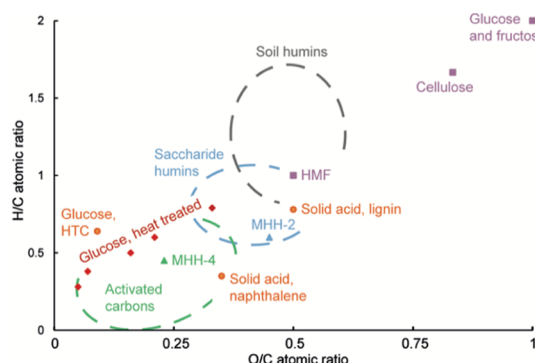

Figure 1. van Krevelen diagram showing microporous humins derived from HMF, saccharide and soil humins, solid acids, HTC of glucose, pyrolysis of glucose, and pure glucose, fructose, cellulose, and HMF (see Table S1). MHH-X denotes microporous humins derived from HMF at 200 and 400 °C.

dehydration product[21−23] of HMF and HMF itself is a dehydration product of fructose/glucose.[24] With the approximate chemical formula of $C_{232}H_{141}O_{105}S$, MHH-2 appeared instead to be a dehydrogenated[25] product of HMF having a reduced H/C ratio. This ratio was consistent with a (partly) aromatic structure. Even though the O/C ratio of MHH-2 was slightly smaller than that of HMF, it does not conclusively exclude that oxidation processes had occurred.[26] A combination of dehydration and dehydrogenation processes could also lead to a reduced O/C ratio. In comparison, solid acids derived from lignin[27] showed higher H/C and O/C ratios than MHH-

2, whereas a solid acid produced from naphthalene[28] displayed a lower ratio. Hydrochars from glucose[29] and humins,[12,30] on the other hand, displayed lower O/C ratios than MHH-2. The carbon content of MHH-2 was higher than those in the solid acids produced from lignin[27] and naphthalene[28] but lower than those in the hydrochars derived from lapsi seeds and glucose.[29,31] The carbon content in MHH-2 compared well with humins but the hydrogen content was lower, except for the product from HMF heated to 190 °C at pH 2.5 (see Table S1), which had comparable values for both carbon and hydrogen contents. Furthermore, 0.69 wt % of sulfur was introduced into MHH-2. This amount was much smaller than that in many other solid acids, which have been shown to contain 3.9−20.0 wt % of sulfur.[27−29] Carbonaceous solids with sulfonic acid-based surface groups, known as sulfonated carbons, are heterogeneous solid acid catalysts. They are typically synthesized by direct and incomplete carbonization or postsynthetic modification of carbonized precursors with H_2SO_4 or other sulfonating agents.[32,33]

The approximate chemical formula of MHH-4 was $C_{470}H_{213}O_{109}S$ (Table S1). Its higher carbon content and lower H/C and O/C atomic ratios than those of MHH-2 indicated a higher degree of aromatization. The carbon content was higher and the hydrogen content was lower than those in typical humins.[34] Its position in the van Krevelen diagram[21] of Figure 1 indicates that it was a dehydration product of HMF. A similar trend for the H/C and O/C atomic ratios, as for the HMF-to-MHH-4 transformation, has been observed for glucose treated with dilute H_2SO_4 and subjecting the formed material to a CO_2 gas mixture and increasing the temperature.[35] In addition, MHH-4 contained even less sulfur than MHH-2 and had a similar oxygen-to-sulfur atomic ratio.

To study the molecular nature of the microporous humins, solid-state cross-polarization (CP) ^{13}C nuclear magnetic resonance (NMR) spectra were recorded for MHH-2. The spectrum in Figure 2 was recorded by using the total suppression of spinning sideband (TOSS) pulse sequence.[36,37] It has broad bands centered at chemical shifts of 128, 153, and 189 ppm. These chemical shifts were assigned to the sp² carbons of aromatic rings, linked $-HC=\underline{C}-O$ in furanic rings or phenols, and carbonyls, respectively. No bands are observed at chemical shifts of 110−118 ppm, corresponding to $C=\underline{C}-$
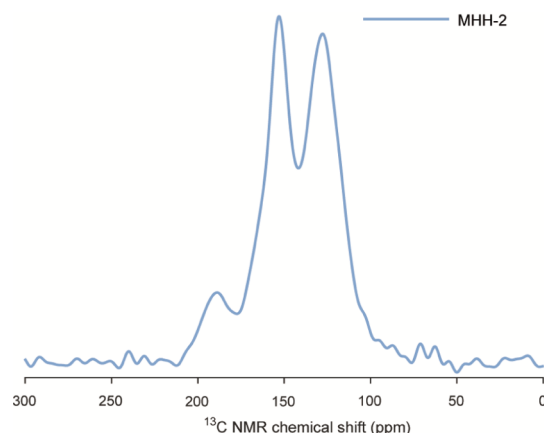

Figure 2. Solid-state cross-polarization ^{13}C nuclear magnetic resonance spectrum of MHH-2 recorded under magic angle spinning with the total suppression of spinning sideband sequence. MHH-2 denotes microporous humin derived from HMF at 200 °C.

C or O−C═CH− in furanic rings.[38,39] Also, the chemical shifts typical for aliphatic ^{13}C are absent, showing that this synthetic procedure was efficient in removing aliphatic carbon typically found in other humins.[30,39] Consistent with the low sulfur content, the typical bands for sulfonated aromatics at chemical shifts of about 140 ppm[40,41] are not observed in Figure 2. Taken all together, the ^{13}C NMR data indicated that MHH-2 was mainly aromatic with oxygen heteroatoms and carbonyl functional groups, likely aldehydes or carboxylic acids, and contained no detectable amounts of aliphatic carbons.

Analyses of the vibrational spectra of MHH-2 and MHH-4 allowed us to identify certain chemical groups and to recognize features of the disordered molecular nature. The Fourier transform infrared (FTIR) spectrum of MHH-2 (Figure S4) has bands at frequencies of 1600 and 1716 cm^{−1}, indicative of C═C and C═O bonds, respectively.[42] The spectrum of MHH-4 have larger relative absorbance of these bands, which are consistent with a larger fraction of aromatic C═C bonds to C═O bonds in MHH-4 than that in MHH-2. The Raman spectra in Figures S5−S8 show typical disordered carbon structures of the bands;[43] however, they varied significantly with the laser power used. Changes occurred in the spectra already at a low laser power of 0.056 mW for the 532 nm laser. Less significant changes were observed in the spectra when using a 785 nm laser. For sample MHH-4, no visible alteration of the spot on the sample that had been irradiated with laser light was observed. The damaging effects of laser irradiation on carbon materials are generally well established.[44,45]

Thermally Stable and Amorphous Structures. The microporous humins displayed relatively high thermal stability in an oxidizing atmosphere. The thermal gravimetric analysis (TGA) traces in Figure S9 were consistent with high stabilities of MHH-2 and MHH-4 up to temperatures of almost 300 °C in air. Certainly, the thermal stabilities were lower than those of typical activated carbons,[15,46] but compared well with the solid acid produced from naphthalene.[28] No ash content was detected after TGA.

As expected, the microporous humins had an amorphous nature as could be deduced from X-ray scattering analysis. The wide-angle X-ray scattering (WAXS) curves for MHH-2 and MHH-4 in Figure 3 are similar with broad peaks centered at 42° and 21° (2θ), respectively. The shoulder peak centered at 10° is slightly more pronounced for MHH-4 than that for MHH-2. The peaks correspond to q = 2.9, 1.5, and 0.7 Å^{−1}. Various analyses of WAXS curves of carbon-rich amorphous solids, including those performed with reverse Monte Carlo routines,[47,48] are consistent with sp[2]-hybridized structures. The
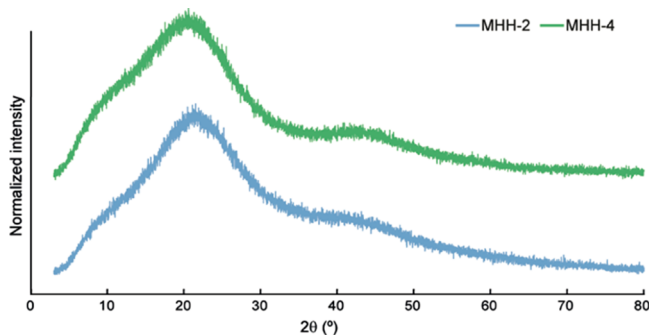
relatively low signal-to-noise ratios of the WAXS data, recorded on an in-house diffractometer, limited the options for quantitative comparisons. Furthermore, the measurements were carried out under ambient conditions and water adsorption is known[49] to shift the peaks to slightly higher q values for activated carbons. Irrespectively, a qualitative discussion of the WAXS curves in Figure 3 is presented below.

The broad peaks and absence of sharp X-ray diffraction peaks[50] in the WAXS curves of MHH-2 and MHH-4 show that they are X-ray amorphous. Disordered aromatic carbon-rich structures are likely responsible for the broad peaks at ∼21 and ∼42° (2θ). For other and possibly related materials, this broadness has been discussed[51] and attributed to, for instance, distorted graphitic structures[52] and carbonaceous structures with differing degrees of crystallinity.[50] Furthermore, the peaks centered at 21° have also been attributed to aliphatic structures in coal,[53] which is inconsistent with our findings from ^{13}C NMR analysis (Figure 2). They have also been attributed to disorder in sp[2] carbons[54] and to stacked aromatic layers with perpendicular crystallites.[55] The shoulder centered at 10° (2θ) or q = 0.7 Å^{−1} is, to the best of our knowledge, not usually discussed for porous aromatic carbonaceous solids such as activated carbons. A peak in that position can result from oxygen functional groups in (and water between) aromatic carbon layers,[56] which is typical for graphite oxide and consistent with our findings from elemental analysis and FTIR and ^{13}C NMR spectroscopy. Furthermore, amorphous solids, similar to graphite oxide and more or less reduced graphite oxide, can exhibit WAXS peaks at similar positions (2θ ≈ 10, 21, and 42°) as observed for MHH-2 and MHH-4.[57−61]

Textural Properties Derived from Gas Adsorption/ Desorption and Scanning Electron Microscopy. As mentioned, MHH-4 was more porous than MHH-2, cf. Table 1, and the corresponding N₂ sorption isotherms in Figure 4 show large and steep uptake of N₂ at low relative
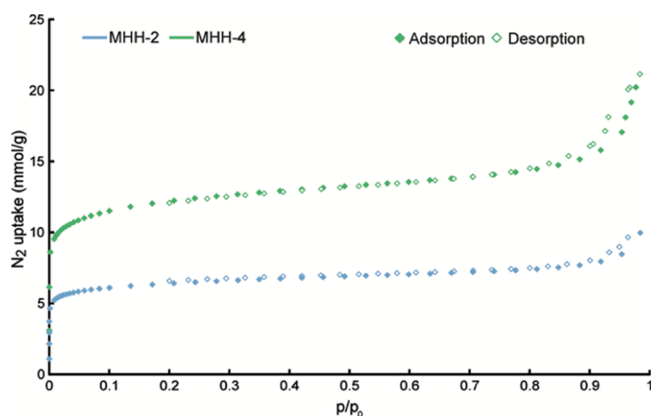
Figure 4. N₂ uptake at −196 °C on microporous humins derived from HMF at 200 and 400 °C (MHH-X).

Figure 3. WAXS curves of microporous humins derived from HMF at 200 and 400 °C (MHH-X).

pressures (p/p₀), which is typical for micropores.[62] They also display an almost linear region of adsorption of N₂ at intermediate levels of p/p₀ and an increased adsorption as p/p₀ approaches 1. The adsorption of N₂ does not reach a plateau for increasingly high values of p/p₀, which indicates that MHH-2 and MHH-4 contained macropores or consisted of small particles.[62,63] The N₂ adsorption/desorption isotherms in Figure 4 show slight hysteresis at p/p₀ of 0.8−1 for both MHH-2 and MHH-4. Hysteresis is typically related to

adsorption metastability, capillary condensation, network effects, swelling, pore blocking, and the shapes of the pores.[62,64] In relation to these N_2 adsorption isotherms, pore size distributions and cumulative pore volumes were calculated using a density functional theory (DFT) method. These are presented in Figures S10 and S11. To estimate the volume of small pores, the Dubinin−Radushkevich (DR) method was used to determine the ultramicropore volumes, using CO_2 sorption data recorded at 0 °C. MHH-4 and MHH-2 had ultramicropore volumes of 0.39 and 0.25 cm^3/g (see Figure S12 and Supporting calculations), respectively. As was expected, the ultramicropore volumes failed to fully agree with the micropore volumes (as was determined with the t-plot method using N_2 adsorption data). CO_2 is effectively smaller than N_2 within sorbents, and the models and the pressure ranges used were different.

The microporous humins consisted of aggregated and interconnected particles with characteristic sizes of 10−100 nm as can be seen from the scanning electron microscopy (SEM) images in Figures 5, S13, and S14. Cavities and
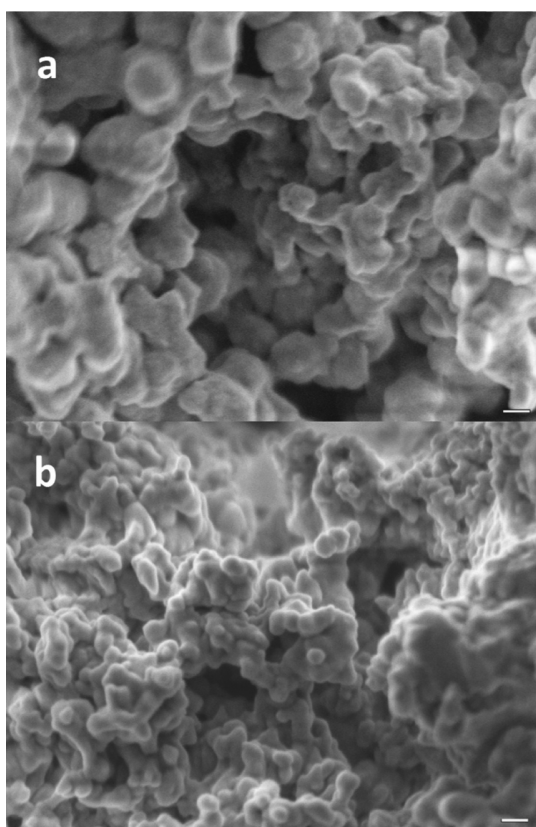
Figure 5. SEM images at 60 000× magnification of microporous humins derived from HMF at (a) 200 and (b) 400 °C (MHH-X). The scale bars at the bottom right of each image correspond to 100 nm.

channels had formed among the aggregated particles, and the interconnections appeared broadly distributed with respect to size and shape. The particle sizes were significantly smaller than the droplet size of the atomized HMF. Tentatively, the small sizes of the particles were assigned to features of the phase separation induced by the addition of diethyl ether. Carbon-rich solids, produced in different manners, such as carbon-coated counter electrodes,[65] fuel cell cathodes,[66]

graphene oxide composites,[67] carbon black,[68] silicon carbide,[69] and soot,[54] have been shown to have comparable morphologies to those seen for MHH-2 and MHH-4. Such small and interconnected particles can, speculatively, enhance the mass transport rates important to various applications. Note that the SEM analyses of MHH-2 and MHH-4 showed charging, which is indicative of low conductivities.[70,71]

Gas Uptake and Selectivity. Compared with porous polymers (Table S3[72−82]), MHH-4 showed the highest reported uptakes of CO_2 at 0.15 bar and 0 °C (2.18 mmol/g), as shown in Figure 6. This low-pressure uptake was also
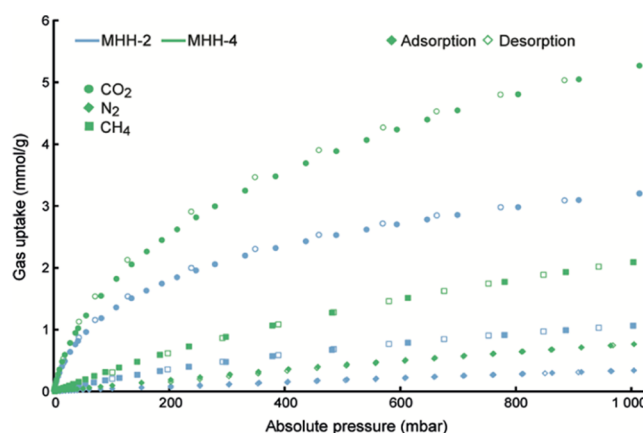
Figure 6. Sorption isotherms recorded at 0 °C for microporous humins derived from HMF at 200 and 400 °C (MHH-X).

comparable to some of the highest uptakes of activated carbons (Table S3). The CO_2 uptake at 1 bar at 0 °C (5.27 mmol/g) was on par with some of the best porous polymers but lower than those of certain activated carbons (Table S3), zeolites, and metal−organic frameworks.[83,84] The uptake of CH_4 was relatively high for MHH-4, with a value of 2.09 mmol/g at 0 °C and 1 bar. For MHH-2, the corresponding uptakes of CO_2 and CH_4 were somewhat lower, with values of 3.20 and 1.06 mmol/g at 0 °C and 1 bar. The CO_2 isotherms for MHH-2 and MHH-4 displayed slight hysteresis at intermediate pressures, which closed on high and low pressures of CO_2. The uptakes of N_2 at 0 °C and 1 bar were 0.34 and 0.77 mmol/g for MHH-2 and MHH-4, respectively. The CO_2 and N_2 sorption isotherms recorded at 50 °C are shown in Figure S15.

Adsorption-driven capture of CO_2 could potentially be less expensive than scrubbing technologies for CO_2 capture and is hence researched for potential implementation.[79] To evaluate the prospects of such capture, it is important to measure or estimate the binary adsorption of CO_2 from gas mixtures. As it is time consuming and experimentally difficult to measure binary adsorption isotherms, various methods have been developed to estimate the binary adsorption from the single-component adsorption data. The ideal adsorption solution theory (IAST)[85] is one of the well-established methods.

The binary selectivites were estimated for the microporous humins with the IAST method, and the CO_2-over-N_2 selectivities in Figure 7a at 0 °C are higher for MHH-4 than that for MHH-2. At p_{tot} = 1 bar, the selectivity increased from 37 up to 65 for MHH-4 on increasing y_{CO_2}. At p_{tot} = 0.1 bar, the selectivity stayed largely independent of y_{CO_2}. We refrain from speculating whether this difference is explained by
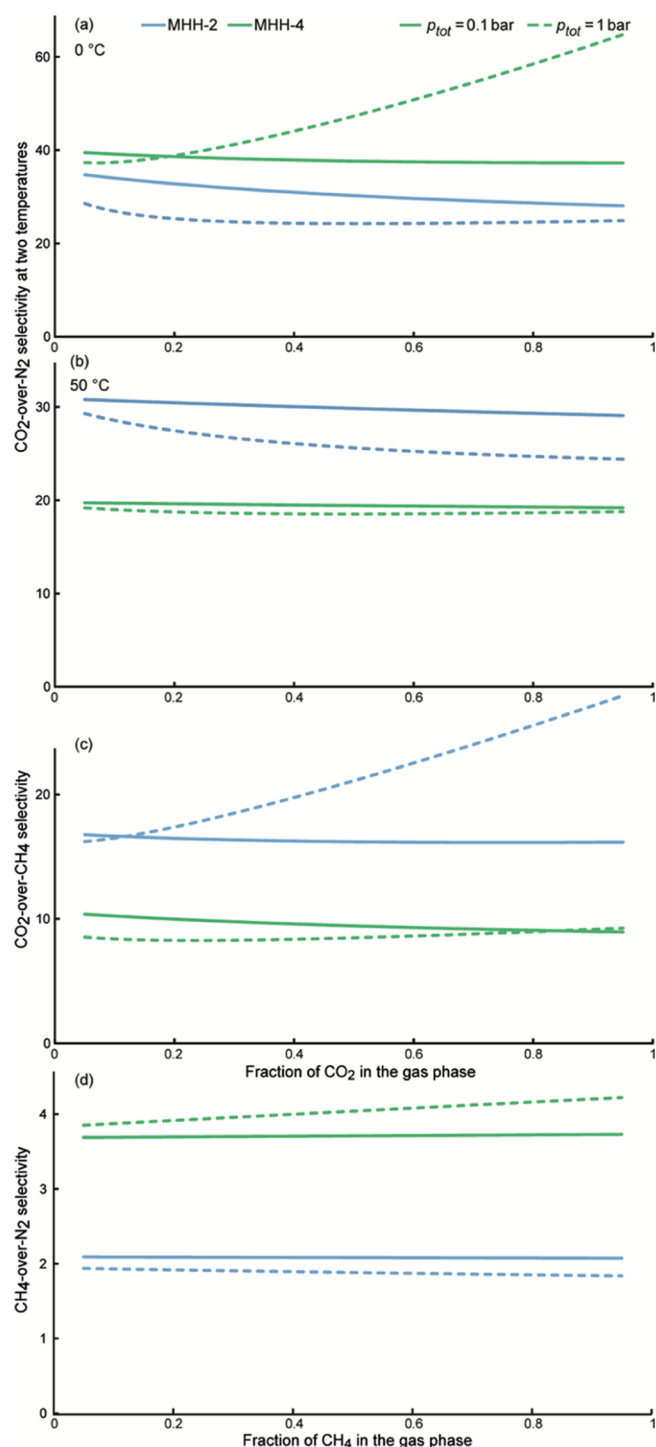
Figure 7. (a,b) CO_2-over-N_2 selectivity at 0 and 50 °C, (c) CO_2-over-CH_4 selectivity, and (d) CH_4-over-N_2 selectivity at 0 °C. IAST was used. MHH-X denotes microporous humins derived from HMF at 200 or 400 °C.

physical reasons or if it is related to the mechanics of the IAST method. IAST has several limitations. These include assumptions of ideal mixing and that the adsorptive uptake of the least interactive gas needs to be integrated over quite a large pressure range, when the selectivity is high. Often, the high-pressure uptake of the least interactive gas is not measured, and hence, regression models are applied to predict the high-pressure adsorption data. Such regression analyses

and integrations were performed for the IAST selectivities of this study. Consequently, the binary selectivities presented in Figure 7 at p_{tot} = 1 bar are less robust than those of 0.1 bar. In contrast to the order observed at a temperature of 0 °C, the selectivity was higher for MHH-2 than that for MHH-4 at a temperature of 50 °C. At p_{tot} = 1 bar and y_{CO_2} = 0.15 (relevant for postcombustion capture of CO_2[83]), the selectivity was ∼19 for MHH-4 (see Figure 7b). MHH-2, on the other hand, had for these $p-T-y_{CO_2}$ conditions a selectivity of ∼28. The selectivities for MHH-2 and MHH-4 were higher than those for most activated carbons. Related values for the CO_2-over-N_2 selectivity for other sorbents have been discussed elsewhere[79,82,86,87] and are presented in Table S3.

Upgraded biogas has the potential to be amongst the most sustainable vehicle fuels[88,89] if the waste biomass and the involved processes are selected with care. The main operation of the upgrading is to remove significant amounts of CO_2. Such CO_2 removal can be performed by, for example, adsorption-driven separation processes.[88] Important properties of the involved sorbents include the CO_2-over-CH_4 selectivity. Hence, the IAST selectivity was calculated from CO_2 and CH_4 adsorption data and presented in Figure 7c as a function of y_{CO_2} at p_{tot} = 0.1 and 1 bar. The selectivity for MHH-4 was ∼10, whereas MHH-2 had higher values of 16−28. In the context of the upgrading of biogas (and landfill gas), y_{CH_4} is typically between 35 and 70% and y_{CO_2} is between 15 and 40%.[90] The reported selectivities of MHH-2 and MHH-4 were larger than those for regular activated carbons but smaller than those of certain carbon molecular sieves and zeolites. The CO_2-over-CH_4 selectivities for other adsorbents have been reviewed or presented elsewhere.[91−93]

The CH_4-over-N_2 selectivity metric is relevant in the context of adsorption-driven upgrading of landfill gas and natural gas, and selectivities for other sorbents have been presented elsewhere.[93,94] This metric was calculated for MHH-2 and MHH-4 by using IAST and CH_4 and N_2 adsorption data and is presented in Figure 7d. The CH_4-over-N_2 selectivity was between 3.8 and 4.2 for MHH-4 and around 2 for MHH-2. See the Supporting Information for further details.

The isosteric heat of the sorption of CO_2 (Q_{st}) is important to adsorption-driven separation of CO_2 from gas mixtures. A high Q_{st} value gives a high CO_2 selectivity. A high Q_{st} value is related to a strong intermolecular interaction of CO_2 with the electrical field gradients (EFGs) of these internal surfaces of the sorbent. Hence, Q_{st} of CO_2 is connected to the pore size as well as the functional groups on the surface.[95,96] However, a high value of Q_{st} also increases the regeneration cost of the sorbent.[97] Hence, for adsorption-driven CO_2 capture from flue gas mixtures, calculations have indicated that Q_{st} of 40−60 kJ/mol could be optimal but other theoretical work has shown vague relationships between Q_{st} and the cost of CO_2 capture operations.[98−100] The loading-dependent Q_{st} values for MHH-2 and MHH-4 were determined with differential methods using temperature- and pressure-dependent CO_2 sorption data and are presented in Figure 8. For MHH-4, Q_{st} was 42−44 kJ/mol, which is significantly higher than those typical for microporous polymers and activated carbons,[78,95,96,101] as presented in Table S3. Q_{st} of MHH-2 was, on the other hand, typical for such sorbents with a value of 30−34 kJ/mol. The loading dependencies were weak. Q_{st} increased slightly for MHH-4 and decreased for MHH-2 with increased loadings.
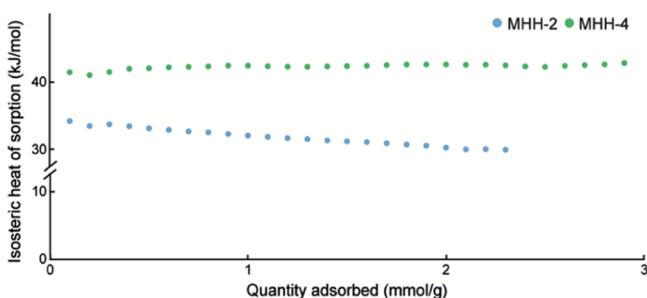
Figure 8. Isoteric heat of sorption of CO_2 for microporous humins derived from HMF at 200 and 400 °C (MHH-X).

This weak dependency indicated a narrow distribution of EFGs, which is consistent with a low heterogeneity of the surface structure.[102,103] The high Q_{st} values for MHH-4 likely result from narrow pores and, to some extent, carbonyl functional groups. (See Supporting Information for calculations and Figures S16−S19 for CO_2 isotherms determined at different temperatures and the corresponding isosteres).

CONCLUSIONS

A new class of highly porous organic sorbents, called microporous humins, was synthesized with a new approach. Tiny droplets of HMF were added rapidly to conc. H_2SO_4 and the formed solids were subsequently treated with diethyl ether and heat. The microporous humins had high Q_{st} values for sorption of CO_2, large Brunauer−Emmett−Teller (BET) surface areas, and micropore volumes. The CO_2-over-N_2, CO_2-over-CH_4, and CH_4-over-N_2 selectivities were high and indicate potential usefulness of the sorbents in gas separation processes. High Q_{st} of sorption of CO_2 for MHH-4 could be relevant to further studies of this composition in relation to CO_2 separation processes. The microporous humins contained aromatic structures with oxygen heteroatoms and carbonyl functional groups and no significant amounts of aliphatic groups. These structures were consistent with dehydration, dehydrogenation, and/or aromatization of HMF. The functional groups could be relevant to further surface modification. Only small amounts of sulfur were included in the sorbents and further studies on how to control the sulfur content or doping with other elements could be warranted. The impact of washing/extraction is seldom studied in the general class of porous polymers and it could be relevant to further studies on the synthesis of microporous humins. We also expect that other molecules than HMF could be polymerized in a similar manner and that the process methodologies could be further refined for upscale purposes. Currently, the cost of HMF is significant but new and improved processes are under the development. This together with the importance of HMF as a reaction intermediate and a potential platform chemical give a considerable potential to develop further the chemistry of HMF, both as a starting material (illustrated by this work) and with HMF as an intermediate.

EXPERIMENTAL SECTION

Synthesis of Sorbents from HMF. HMF (0.63 g) was heated to 50 °C and subsequently atomized as tiny droplets (typically 30−100 μm in size, according to the supplier of the device) and added to 10 mL of conc. H_2SO_4 under vigorous stirring at a temperature of 50 °C. The mixture was kept under vigorous stirring at this temperature for 24 h and subsequently cooled down to room temperature. Diethyl ether was thereafter added carefully under stirring to a total volume of 50 mL, while being cooled in a water bath. The resulting suspension was centrifuged, and the liquid phase was decanted. The procedure of adding diethyl ether and removing the liquid phase was repeated twice. The sorbents were dried in a flow of N_2 and subsequently heated to temperatures of 200 or 400 °C, also in a flow of N_2. The yields were calculated by dividing the solid mass after heat treatment by the initial mass of HMF. All reagents were of a high-purity grade and used as supplied, unless otherwise stated.

Characterization. For elemental analysis, combustion analysis was used, and the samples were assumed to consist entirely of C, H, N, O, and S. The mass of O was calculated by subtraction.

Solid-state CP ^{13}C NMR spectra of MHH-2 (Figures 2 and S3) were recorded under conditions of magic angle spinning (MAS) using the TOSS sequence. A Bruker AVANCE III spectrometer operating at a frequency of 400 MHz for a frequency of 100.6 MHz for ^{13}C was used and a 7 mm probe head was used. The MAS rate was 7 kHz, and the contributions from ^{1}H magnetization were lessened by decoupling with 50 kHz during the acquisition of the ^{13}C signals. Ramped CP for 1.6 ms was used to transfer magnetization to ^{13}C from ^{1}H.

A Varian 670-IR spectrometer with a Specac Goldengate attenuated total reflection device was used to record the FTIR spectra. It was equipped with a room-temperature deuterated triglycine sulfate detector.

Raman spectra were recorded with a HORIBA LabRAM HR 800 Raman spectrometer equipped with a double-frequency neodymium-doped yttrium−aluminum−garnet laser (532 nm/ 50 mW) and an intracavity-regulated laser diode with point source (785 nm/100 mW). The intensity of the lasers was adjusted by using a software-controlled filter wheel with six neutral density filters.

A PerkinElmer TGA 7 device was used for TGA in a flow of dry air. Approximately 3 mg of the sample in a platinum cup was placed inside of the instrument and the weight was allowed to stabilize. Thereafter, the temperature was raised by 1 °C/ min, from 27−900 °C, and the weight was recorded.

A PANalytical X'Pert alpha1 powder diffractometer was used to record WAXS data from $2\theta = 3.0°−80°$ in a reflection mode with a PIXcel detector (Cu Kα1 radiation, $k = 1.5406$ Å). The q-values were calculated according to $q = (4\pi/k)\ \sin(2\theta/2)$.

SEM images were recorded using a JEOL JSM-7401F microscope equipped with an in-lens secondary-electron column detector. A "gentle beam" mode was used with a negative bias (−2 kV) applied on the sample stage and a column accelerating voltage of 3 kV, generating a landing energy corresponding to 1 kV. The powders were fixated by using an ink. A working distance of 1.5 mm was used.

Adsorption and desorption isotherms were measured in an absolute pressure range of 0−101 kPa using a Micromeritics ASAP 2020 device. Prior to sorption measurements, the samples were degassed at a temperature of 200 or 400 °C under conditions of dynamic vacuum for 6 h N_2 sorption isotherms were measured at temperatures of −196, 0, and 50 °C. CO_2 sorption isotherms were measured at temperatures of 0, 10, 20, and 50 °C. CH_4 sorption isotherms were measured at a temperature of 0 °C. The BET[104] model was used to calculate the specific surface areas (S_{BET}) using the low-temperature (−196 °C) N_2 uptake at p/p_0 values of 0−0.084

for MHH-4 and 0−0.06 for MHH-2. The selected pressure range assured that $n(1 − p/p_0)$ increased with p/p_0 and that the BET parameter c was positive. The t-plot method (for carbon black and $p/p_0 = 0.2$−0.5) was used to determine S_{ext} and V_{mic}. S_{mic} was calculated as the difference between S_{BET} and S_{ext}.[105,106] V_t was determined at $p/p_0 = 0.98$. Details regarding the calculations can be found in the Supporting Information. A DFT-based method, supplied by Micromeritics routines, was used to estimate pore size distributions using the N_2 adsorption data recorded at a temperature of −196 °C. The ultramicropore volumes were determined using the DR method and CO_2 adsorption data at a temperature of 0 °C, see Supporting Information for details. The IAST was used to calculate binary selectivity from single-component adsorption data, see the Supporting Information for details. CO_2 sorption isotherms were recorded at a temperature of 0 °C on Micromeritics Gemini VII to verify the reproducibility of the synthesis.

■ ASSOCIATED CONTENT

Ⓢ Supporting Information

The Supporting Information is available free of charge on the ACS Publications website at DOI: 10.1021/acsomega.8b01274.

> Sorption isotherms; NMR, FTIR, and Raman spectra; TGA curves; DFT-calculated pore volumes and sizes; DR plot, SEM images, sorption isosters; t-plots; elemental compositions; gas uptake and apparent selectivities; CO_2 uptake, selectivity, and heat of adsorption comparison; IAST data; heat of sorption; and calculations of t-plot, BET, total pore volume, IAST, heat of sorption, and DR micropore volume (PDF)

■ AUTHOR INFORMATION

Corresponding Author
*E-mail: niklas.hedin@mmk.su.se (N.H.).
ORCID Ⓘ
Diana Bernin: 0000-0002-9611-2263
Niklas Hedin: 0000-0002-7284-2974
Present Address
†Department of Chemistry and Chemical Engineering, Chalmers University of Technology, SE-41296 Gothenburg, Sweden.

Notes
The authors declare the following competing financial interest(s): NH co-funded SIA NeoZeo that is commercializing biogas upgrading

■ ACKNOWLEDGMENTS

■ REFERENCES

(1) Dolores, L.-C.; Juan, P. M.-L.; Falco, C.; Titirici, M.-M.; Diego, C.-A. Sustainable Carbon Materials from Hydrothermal Processes; John Wiley & Sons: Oxford, 2013.

(2) Titirici, M.-M.; White, R. J.; Brun, N.; Budarin, V. L.; Su, D. S.; del Monte, F.; Clark, J. H.; MacLachlan, M. J. Sustainable Carbon Materials. Chem. Soc. Rev. 2015, 44, 250−290.

(3) White, R. J.; Budarin, V.; Luque, R.; Clark, J. H.; Macquarrie, D. J. Tuneable Porous Carbonaceous Materials from Renewable Resources. Chem. Soc. Rev. 2009, 38, 3401−3418.

(4) Girisuta, B.; Janssen, L. P. B. M.; Heeres, H. J. A Kinetic Study on the Decomposition of 5-Hydroxymethylfurfural into Levulinic Acid. Green Chem. 2006, 8, 701.

(5) Esposito, D.; Antonietti, M. Redefining Biorefinery: The Search for Unconventional Building Blocks for Materials. Chem. Soc. Rev. 2015, 44, 5821−5835.

(6) Teong, S. P.; Yi, G.; Zhang, Y. Hydroxymethylfurfural Production from Bioresources: Past, Present and Future. Green Chem. 2014, 16, 2015.

(7) Climent, M. J.; Corma, A.; Iborra, S. Conversion of Biomass Platform Molecules into Fuel Additives and Liquid Hydrocarbon Fuels. Green Chem. 2014, 16, 516−547.

(8) van Putten, R.-J.; van der Waal, J. C.; de Jong, E.; Rasrendra, C. B.; Heeres, H. J.; de Vries, J. G. Hydroxymethylfurfural, a Versatile Platform Chemical Made from Renewable Resources. Chem. Rev. 2013, 113, 1499−1597.

(9) Titirici, M.-M.; Antonietti, M. Chemistry and Materials Options of Sustainable Carbon Materials Made by Hydrothermal Carbonization. Chem. Soc. Rev. 2010, 39, 103−116.

(10) Mija, A.; van der Waal, J. C.; van Klink, G.; de Jong, E. Humins-Containing Foam. WO 2017/074183 A1, 2016.

(11) Love, R. M. Spectroscopic studies of carbohydrates. 1. The action of sulphuric acid on sugars. Biochem. J. 1953, 55, 126−132.

(12) Sumerskii, I. V.; Krutov, S. M.; Zarubin, M. Y. Humin-like Substances Formed under the Conditions of Industrial Hydrolysis of Wood. Russ. J. Appl. Chem. 2010, 83, 320−327.

(13) Dias, J. M.; Alvim-Ferraz, M. C. M.; Almeida, M. F.; Rivera-Utrilla, J.; Sánchez-Polo, M. Waste Materials for Activated Carbon Preparation and Its Use in Aqueous-Phase Treatment: A Review. J. Environ. Manage. 2007, 85, 833−846.

(14) Kim, D.-Y.; Nishiyama, Y.; Wada, M.; Kuga, S. High-Yield Carbonization of Cellulose by Sulfuric Acid Impregnation. Cellulose 2001, 8, 29−33.

(15) Ryoo, R.; Joo, S. H.; Jun, S. Synthesis of Highly Ordered Carbon Molecular Sieves via Template-Mediated Structural Transformation. J. Phys. Chem. B 1999, 103, 7743−7746.

(16) Zhou, Z.; Zhao, X. S.; Zeng, X. T. Surface Patterning with Carbon Thin Films by Nanosphere Lithography. Surf. Coat. Technol. 2005, 198, 178−183.

(17) Alatalo, S.-M.; Pileidis, F.; Mäkilä, E.; Sevilla, M.; Repo, E.; Salonen, J.; Sillanpää, M.; Titirici, M.-M. Versatile Cellulose-Based Carbon Aerogel for the Removal of Both Cationic and Anionic Metal Contaminants from Water. ACS Appl. Mater. Interfaces 2015, 7, 25875−25883.

(18) Hu, Y.; Yang, J.; Tian, J.; Jia, L.; Yu, J.-S. Waste Frying Oil as a Precursor for One-Step Synthesis of Sulfur-Doped Carbon Dots with PH-Sensitive Photoluminescence. Carbon 2014, 77, 775−782.

(19) Rabbani, M. G.; El-Kaderi, H. M. Synthesis and Characterization of Porous Benzimidazole-Linked Polymers and Their Performance in Small Gas Storage and Selective Uptake. Chem. Mater. 2012, 24, 1511−1517.

(20) Xu, Y.; Jin, S.; Xu, H.; Nagai, A.; Jiang, D. Conjugated Microporous Polymers: Design, Synthesis and Application. Chem. Soc. Rev. 2013, 42, 8012−8031.

(21) Van Krevelen, D. W. Graphical Statistical Method for the Study of Structure and Reaction Processes of Coal. Fuel 1950, 29, 269−284.

(22) Sevilla, M.; Fuertes, A. B. The Production of Carbon Materials by Hydrothermal Carbonization of Cellulose. Carbon 2009, 47, 2281−2289.

(23) Sevilla, M.; Fuertes, A. B. Chemical and Structural Properties of Carbonaceous Products Obtained by Hydrothermal Carbonization of Saccharides. Chem.—Eur. J. 2009, 15, 4195−4203.

(24) Rosatella, A. A.; Simeonov, S. P.; Frade, R. F. M.; Afonso, C. A. M. 5-Hydroxymethylfurfural (HMF) as a Building Block Platform: Biological Properties, Synthesis and Synthetic Applications. Green Chem. 2011, 13, 754.

(25) Klavins, M.; Purmalis, O. Genesis of Peat Humic Acid Structure and Properties Within Bog Profile. *Functions of Natural Organic Matter in Changing Environment*; Xu, J., Wu, J., He, Y., Eds.; Springer Netherlands: Dordrecht, 2013; pp 101−105.

(26) Kroll, J. H.; Donahue, N. M.; Jimenez, J. L.; Kessler, S. H.; Canagaratna, M. R.; Wilson, K. R.; Altieri, K. E.; Mazzoleni, L. R.; Wozniak, A. S.; Bluhm, H.; et al. Carbon oxidation state as a metric for describing the chemistry of atmospheric organic aerosol. *Nat. Chem.* **2011**, *3*, 133−139.

(27) Guo, F.; Xiu, Z.-L.; Liang, Z.-X. Synthesis of Biodiesel from Acidified Soybean Soapstock Using a Lignin-Derived Carbonaceous Catalyst. *Appl. Energy* **2012**, *98*, 47−52.

(28) Hara, M.; Yoshida, T.; Takagaki, A.; Takata, T.; Kondo, J. N.; Hayashi, S.; Domen, K. A Carbon Material as a Strong Protonic Acid. *Angew. Chem., Int. Ed.* **2004**, *43*, 2955−2958.

(29) Liang, X.; Yang, J. Synthesis of a Novel Carbon Based Strong Acid Catalyst through Hydrothermal Carbonization. *Catal. Lett.* **2009**, *132*, 460−463.

(30) Van Zandvoort, I.; Wang, Y.; Rasrendra, C. B.; Van Eck, E. R. H.; Bruijnincx, P. C. A.; Heeres, H. J.; Weckhuysen, B. M. Formation, Molecular Structure, and Morphology of Humins in Biomass Conversion: Influence of Feedstock and Processing Conditions. *ChemSusChem* **2013**, *6*, 1745−1758.

(31) Shrestha, R. M.; Varga, I.; Bajtai, J.; Varga, M. Design of Surface Functionalization of Waste Material Originated Charcoals by an Optimized Chemical Carbonization for the Purpose of Heavy Metal Removal from Industrial Waste Waters. *Microchem. J.* **2013**, *108*, 224−232.

(32) Kang, S.; Ye, J.; Chang, J. Recent Advances in Carbon-Based Sulfonated Catalyst: Preparation and Application. *Int. Rev. Chem. Eng.* **2013**, *5*, 133−144.

(33) Nakajima, K.; Hara, M. Amorphous Carbon with SO3H Groups as a Solid Brønsted Acid Catalyst. *ACS Catal.* **2012**, *2*, 1296−1304.

(34) Girisuta, B.; Janssen, L. P. B. M.; Heeres, H. J. Kinetic Study on the Acid-Catalyzed Hydrolysis of Cellulose to Levulinic Acid. *Ind. Eng. Chem. Res.* **2007**, *46*, 1696−1708.

(35) Hoang, T. M. C.; van Eck, E. R. H.; Bula, W. P.; Gardeniers, J. G. E.; Lefferts, L.; Seshan, K. Humin Based By-Products from Biomass Processing as a Potential Carbonaceous Source for Synthesis Gas Production. *Green Chem.* **2015**, *17*, 959−972.

(36) Dixon, W. T. Spinning-sideband-free and spinning-sideband-only NMR spectra in spinning samples. *J. Chem. Phys.* **1982**, *77*, 1800−1809.

(37) Dixon, W. T.; Schaefer, J.; Sefcik, M. D.; Stejskal, E. O.; McKay, R. A. Total Suppression of Sidebands in CPMAS C-13 NMR. *J. Magn. Reson.* **1982**, *49*, 341−345.

(38) Falco, C.; Baccile, N.; Titirici, M.-M. Morphological and Structural Differences between Glucose, Cellulose and Lignocellulosic Biomass Derived Hydrothermal Carbons. *Green Chem.* **2011**, *13*, 3273.

(39) van Zandvoort, I.; Koers, E. J.; Weingarth, M.; Bruijnincx, P. C. A.; Baldus, M.; Weckhuysen, B. M. Structural characterization of 13C-enriched humins and alkali-treated 13C humins by 2D solid-state NMR. *Green Chem.* **2015**, *17*, 4383−4392.

(40) Moujahid, E. M.; Inacio, J.; Besse, J.-P.; Leroux, F. Adsorption of Styrene Sulfonate vs. Polystyrene Sulfonate on Layered Double Hydroxides. *Microporous Mesoporous Mater.* **2003**, *57*, 37−46.

(41) Nakajima, K.; Tomita, I.; Hara, M.; Hayashi, S.; Domen, K.; Kondo, J. N. A Stable and Highly Active Hybrid Mesoporous Solid Acid Catalyst. *Adv. Mater.* **2005**, *17*, 1839−1842.

(42) Sun, X.; Li, Y. Colloidal Carbon Spheres and Their Core/Shell Structures with Noble-Metal Nanoparticles. *Angew. Chem., Int. Ed.* **2004**, *43*, 597−601.

(43) Merlen, A.; Buijnsters, J.; Pardanaud, C. A Guide to and Review of the Use of Multiwavelength Raman Spectroscopy for Characterizing Defective Aromatic Carbon Solids: From Graphene to Amorphous Carbons. *Coatings* **2017**, *7*, 153.

(44) Ferrari, A. C.; Robertson, J. Resonant Raman Spectroscopy of Disordered, Amorphous, and Diamondlike Carbon. *Phys. Rev. B: Condens. Matter Mater. Phys.* **2001**, *64*, 075414.

(45) Kundu, A.; Rani, R.; Hazra, K. S. Graphene Oxide Demonstrates Experimental Confirmation of Abraham Pressure on Solid Surface. *Sci. Rep.* **2017**, *7*, 42538.

(46) Rychlicki, G.; Terzyk, A. P.; Majchrzycki, W. The Effect of Commercial Carbon De-Ashing on Its Thermal Stability and Porosity. *J. Chem. Technol. Biotechnol.* **1999**, *74*, 329−336.

(47) Jain, S. K.; Pellenq, R. J.-M.; Gubbins, K. E. Structural Modeling of Porous Carbons Using a Hybrid Reverse Monte Carlo Method. *Adsorption* **2007**, *3*, 129−137.

(48) Jain, S. K.; Pellenq, R. J.-M.; Pikunic, J. P.; Gubbins, K. E. Molecular Modeling of Porous Carbons Using the Hybrid Reverse Monte Carlo Method. *Langmuir* **2006**, *22*, 9942−9948.

(49) László, K.; Czakkel, O.; Dobos, G.; Lodewyckx, P.; Rochas, C.; Geissler, E. Water Vapour Adsorption in Highly Porous Carbons as Seen by Small and Wide Angle X-Ray Scattering. *Carbon* **2010**, *48*, 1038−1048.

(50) Omri, A.; Benzina, M.; Ammar, N. Preparation, Modification and Industrial Application of Activated Carbon from Almond Shell. *J. Ind. Eng. Chem.* **2013**, *19*, 2092−2099.

(51) Marsh, H.; Rodríguez-Reinoso, F. *Activated Carbon*; Elsevier: Amsterdam, 2006.

(52) Pechyen, C.; Atong, D.; Aht-Ong, D.; Sricharoenchaikul, V. Investigation of Pyrolyzed Chars from Physic Nut Waste for the Preparation of Activated Carbon. *J. Solid Mech. Mater. Eng.* **2007**, *1*, 498−507.

(53) Sonibare, O. O.; Haeger, T.; Foley, S. F. Structural Characterization of Nigerian Coals by X-Ray Diffraction, Raman and FTIR Spectroscopy. *Energy* **2010**, *35*, 5347−5353.

(54) Mohan, A. N.; Manoj, B. Synthesis and Characterization of Carbon Nanospheres from Hydrocarbon Soot. *Int. J. Electrochem. Sci.* **2012**, *7*, 9537−9549.

(55) Takagi, H.; Maruyama, K.; Yoshizawa, N.; Yamada, Y.; Sato, Y. XRD Analysis of Carbon Stacking Structure in Coal during Heat Treatment. *Fuel* **2004**, *83*, 2427−2433.

(56) Thakur, S.; Karak, N. Green Reduction of Graphene Oxide by Aqueous Phytoextracts. *Carbon* **2012**, *50*, 5331−5339.

(57) Park, S.; An, J.; Potts, J. R.; Velamakanni, A.; Murali, S.; Ruoff, R. S. Hydrazine-Reduction of Graphite- and Graphene Oxide. *Carbon* **2011**, *49*, 3019−3023.

(58) Blanton, T. N.; Majumdar, D. Characterization of X-Ray Irradiated Graphene Oxide Coatings Using X-Ray Diffraction, X-Ray Photoelectron Spectroscopy, and Atomic Force Microscopy. *Powder Diffr.* **2013**, *28*, 68−71.

(59) Blanton, T. N.; Majumdar, D. X-Ray Diffraction Characterization of Polymer Intercalated Graphite Oxide. *Powder Diffr.* **2012**, *27*, 104−107.

(60) Mu, S.-J.; Su, Y.-C.; Xiao, L.-H.; Liu, S.-D.; Hu, T.; Tang, H.-B. X-Ray Difraction Pattern of Graphite Oxide. *Chin. Phys. Lett.* **2013**, *30*, 096101.

(61) Loryuenyong, V.; Totepvimarn, K.; Eimburanapravat, P.; Boonchompoo, W.; Buasri, A. Preparation and Characterization of Reduced Graphene Oxide Sheets via Water-Based Exfoliation and Reduction Methods. *Adv. Mater. Sci. Eng.* **2013**, *2013*, 1−5.

(62) Thommes, M.; Kaneko, K.; Neimark, A. V.; Olivier, J. P.; Rodriguez-Reinoso, F.; Rouquerol, J.; Sing, K. S. W. Physisorption of Gases, with Special Reference to the Evaluation of Surface Area and Pore Size Distribution. *Pure Appl. Chem.* **2015**, *87*, 1051−1069.

(63) Leofanti, G.; Padovan, M.; Tozzola, G.; Venturelli, B. Surface Area and Pore Texture of Catalysts. *Catal. Today* **1998**, *41*, 207−219.

(64) Sing, K. The Use of Nitrogen Adsorption for the Characterisation of Porous Materials. *Colloids Surf., A* **2001**, *187−188*, 3−9.

(65) Murakami, T. N.; Ito, S.; Wang, Q.; Nazeeruddin, M. K.; Bessho, T.; Cesar, I.; Liska, P.; Humphry-Baker, R.; Comte, P.; Péchy, P.; et al. Highly Efficient Dye-Sensitized Solar Cells Based on Carbon Black Counter Electrodes. *J. Electrochem. Soc.* **2006**, *153*, A2255.

(66) Liu, Z. Y.; Brady, B. K.; Carter, R. N.; Litteer, B.; Budinski, M.; Hyun, J. K.; Muller, D. A. Characterization of Carbon Corrosion-Induced Structural Damage of PEM Fuel Cell Cathode Electrodes Caused by Local Fuel Starvation. *J. Electrochem. Soc.* **2008**, *155*, B979−B984.

(67) Silva, A. M. T.; Fonseca, N. N. C.; Vaz, J. R.; Figueiredo, J. L.; Faria, J. L. Photocatalytic Reduction of CO2 with Water into Methanol and Ethanol Using Graphene Derivative − TiO2 Composites: Effect of PH and Copper (I) Oxide. *Top. Catal.* **2016**, *59*, 1279−1291.

(68) Li, X.; Li, X.; Banis, M. N.; Wang, B.; Lushington, A.; Cui, X.; Li, R.; Sham, T.-K.; Sun, X. Tailoring interactions of carbon and sulfur in Li-S battery cathodes: significant effects of carbon-heteroatom bonds. *J. Mater. Chem. A* **2014**, *2*, 12866.

(69) van Laar, J. H.; van der Walt, I. J.; Bissett, H.; Puts, G. J.; Crouse, P. L. Synthesis and deposition of silicon carbide nanopowders in a microwave-induced plasma operating at low to atmospheric pressures. *J. South. Afr. Inst. Min. Metall.* **2015**, *115*, 949−955.

(70) Park, J. B.; Kim, Y.-J.; Yoo, J. M.; Kim, Y.; Kim, S. M.; Kim, S. J.; Gorbachev, R.; Barbolina, I. I.; Yoon, J. M.; Hee, B. H.; et al. Non-Destructive Electron Microscopy Imaging and Analysis of Biological Samples with Graphene Coating. *2D Materials* **2016**, *3*, 045004.

(71) Scipioni, R.; Jørgensen, P. S.; Ngo, D.-T.; Simonsen, S. B.; Liu, Z.; Yakal-Kremski, K. J.; Wang, H.; Hjelm, J.; Norby, P.; Barnett, S. A.; et al. Electron microscopy investigations of changes in morphology and conductivity of LiFePO 4 /C electrodes. *J. Power Sources* **2016**, *307*, 259−269.

(72) Hao, W.; Björnerbäck, F.; Trushkina, Y.; Oregui Bengoechea, M.; Salazar-Alvarez, G.; Barth, T.; Hedin, N. High-Performance Magnetic Activated Carbon from Solid Waste from Lignin Conversion Processes. 1. Their Use As Adsorbents for CO2. *ACS Sustainable Chem. Eng.* **2017**, *5*, 3087−3095.

(73) Sevilla, M.; Falco, C.; Titirici, M.-M.; Fuertes, A. B. High-Performance CO2 Sorbents from Algae. *RSC Adv.* **2012**, *2*, 12792.

(74) Wahby, A.; Ramos-Fernández, J. M.; Martínez-Escandell, M.; Sepúlveda-Escribano, A.; Silvestre-Albero, J.; Rodríguez-Reinoso, F. High-Surface-Area Carbon Molecular Sieves for Selective CO2 Adsorption. *ChemSusChem* **2010**, *3*, 974−981.

(75) Sevilla, M.; Fuertes, A. B. Sustainable porous carbons with a superior performance for CO2 capture. *Energy Environ. Sci.* **2011**, *4*, 1765.

(76) Creamer, A. E.; Gao, B. Carbon-Based Adsorbents for Postcombustion CO2 Capture: A Critical Review. *Environ. Sci. Technol.* **2016**, *50*, 7276−7289.

(77) Lee, S.-Y.; Park, S.-J. A Review on Solid Adsorbents for Carbon Dioxide Capture. *J. Ind. Eng. Chem.* **2015**, *23*, 1−11.

(78) Wang, W.; Zhou, M.; Yuan, D. Carbon Dioxide Capture in Amorphous Porous Organic Polymers. *J. Mater. Chem. A* **2017**, *5*, 1334−1347.

(79) Samanta, A.; Zhao, A.; Shimizu, G. K. H.; Sarkar, P.; Gupta, R. Post-Combustion CO2 Capture Using Solid Sorbents: A Review. *Ind. Eng. Chem. Res.* **2012**, *51*, 1438−1463.

(80) Deng, S.; Wei, H.; Chen, T.; Wang, B.; Huang, J.; Yu, G. Superior CO2 Adsorption on Pine Nut Shell-Derived Activated Carbons and the Effective Micropores at Different Temperatures. *Chem. Eng. J.* **2014**, *253*, 46−54.

(81) Alabadi, A.; Razzaque, S.; Yang, Y.; Chen, S.; Tan, B. Highly porous activated carbon materials from carbonized biomass with high CO 2 capturing capacity. *Chem. Eng. J.* **2015**, *281*, 606−612.

(82) Xu, C.; Hedin, N. Microporous adsorbents for CO2 capture - a case for microporous polymers? *Mater. Today* **2014**, *17*, 397−403.

(83) Sayari, A.; Belmabkhout, Y.; Serna-Guerrero, R. Flue Gas Treatment via CO2 Adsorption. *Chem. Eng. J.* **2011**, *171*, 760−774.

(84) Cheung, O.; Hedin, N. Zeolites and Related Sorbents with Narrow Pores for CO2 Separation from Flue Gas. *RSC Adv.* **2014**, *4*, 14480−14494.

(85) Myers, A. L.; Prausnitz, J. M. Thermodynamics of Mixed-Gas Adsorption. *AIChE J.* **1965**, *11*, 121−127.

(86) Yu, C.-H.; Huang, C.-H.; Tan, C.-S. A Review of CO2 Capture by Absorption and Adsorption. *Aerosol Air Qual. Res.* **2012**, *12*, 745−769.

(87) Li, J.-R.; Ma, Y.; McCarthy, M. C.; Sculley, J.; Yu, J.; Jeong, H.-K.; Balbuena, P. B.; Zhou, H.-C. Carbon Dioxide Capture-Related Gas Adsorption and Separation in Metal-Organic Frameworks. *Coord. Chem. Rev.* **2011**, *255*, 1791−1823.

(88) Grande, C. A. *Biofuel's Engineering Process Technology*; Dos Santos Bernardes, M. A., Ed.; InTech, 2011.

(89) Edwards, R.; Larive, J.-F.; Rickeard, D.; Weindorf, W. *Well-to-Tank Version 4 JEC Well-to-Wheels Analysis*, Luxembourg, 2013.

(90) Sun, Q.; Li, H.; Yan, J.; Liu, L.; Yu, Z.; Yu, X. Selection of Appropriate Biogas Upgrading Technology-a Review of Biogas Cleaning, Upgrading and Utilisation. *Renewable Sustainable Energy Rev.* **2015**, *51*, 521−532.

(91) Chaemchuen, S.; Kabir, N. A.; Zhou, K.; Verpoort, F. Metal-Organic Frameworks for Upgrading Biogas via CO2 Adsorption to Biogas Green Energy. *Chem. Soc. Rev.* **2013**, *42*, 9304−9332.

(92) Nugent, P.; Belmabkhout, Y.; Burd, S. D.; Cairns, A. J.; Luebke, R.; Forrest, K.; Pham, T.; Ma, S.; Space, B.; Wojtas, L.; et al. Porous Materials with Optimal Adsorption Thermodynamics and Kinetics for CO2 Separation. *Nature* **2013**, *495*, 80−84.

(93) Yuan, B.; Wu, X.; Chen, Y.; Huang, J.; Luo, H.; Deng, S. Adsorption of CO2, CH4, and N2 on Ordered Mesoporous Carbon: Approach for Greenhouse Gases Capture and Biogas Upgrading. *Environ. Sci. Technol.* **2013**, *47*, 5474−5480.

(94) Ren, X.; Sun, T.; Hu, J.; Wang, S. Highly Enhanced Selectivity for the Separation of CH4 over N2 on Two Ultra-Microporous Frameworks with Multiple Coordination Modes. *Microporous Mesoporous Mater.* **2014**, *186*, 137−145.

(95) Himeno, S.; Komatsu, T.; Fujita, S. High-Pressure Adsorption Equilibria of Methane and Carbon Dioxide on Several Activated Carbons. *J. Chem. Eng. Data* **2005**, *50*, 369−376.

(96) Dawson, R.; Adams, D. J.; Cooper, A. I. Chemical Tuning of CO2 Sorption in Robust Nanoporous Organic Polymers. *Chem. Sci.* **2011**, *2*, 1173.

(97) Dawson, R.; Stöckel, E.; Holst, J. R.; Adams, D. J.; Cooper, A. I. Microporous Organic Polymers for Carbon Dioxide Capture. *Energy Environ. Sci.* **2011**, *4*, 4239.

(98) Hasan, M. M. F.; First, E. L.; Floudas, C. A. Cost-Effective CO2 Capture Based on in Silico Screening of Zeolites and Process Optimization. *Phys. Chem. Chem. Phys.* **2013**, *15*, 17601.

(99) Lin, L.-C.; Berger, A. H.; Martin, R. L.; Kim, J.; Swisher, J. A.; Jariwala, K.; Rycroft, C. H.; Bhown, A. S.; Deem, M. W.; Haranczyk, M.; et al. In Silico Screening of Carbon-Capture Materials. *Nat. Mater.* **2012**, *11*, 633−641.

(100) Huck, J. M.; Lin, L.-C.; Berger, A. H.; Shahrak, M. N.; Martin, R. L.; Bhown, A. S.; Haranczyk, M.; Reuter, K.; Smit, B. Evaluating different classes of porous materials for carbon capture. *Energy Environ. Sci.* **2014**, *7*, 4132−4146.

(101) Lu, W.; Yuan, D.; Sculley, J.; Zhao, D.; Krishna, R.; Zhou, H.-C. Sulfonate-Grafted Porous Polymer Networks for Preferential CO2Adsorption at Low Pressure. *J. Am. Chem. Soc.* **2011**, *133*, 18126−18129.

(102) Belmabkhout, Y.; Sayari, A. Effect of pore expansion and amine functionalization of mesoporous silica on CO2 adsorption over a wide range of conditions. *Adsorption* **2009**, *15*, 318−328.

(103) Rege, S. U.; Yang, R. T.; Buzanowski, M. A. Sorbents for Air Prepurification in Air Separation. *Chem. Eng. Sci.* **2000**, *55*, 4827−4838.

(104) Brunauer, S.; Emmett, P. H.; Teller, E. Adsorption of Gases in Multimolecular Layers. *J. Am. Chem. Soc.* **1938**, *60*, 309−319.

(105) Lowell, S.; Shields, J. E.; Thomas, M. A.; Thommes, M. *Characterization of Porous Solids and Powders: Surface Area, Pore Size and Density*; Springer, 2004; Vol. *16*.

(106) ASTM International. *Standard Test Method for Carbon Black—Total and External Surface Area by Nitrogen*, 2012; Vol. D6556.